Article

Path Loss Model for Outdoor Parking Environments at 28 GHz and 38 GHz for 5G Wireless Networks

Ahmed M. Al-Samman [1],*, Tharek Abd Rahman [1], MHD Nour Hindia [2], Abdusalama Daho [1] and Effariza Hanafi [2]

[1] Wireless Communication Center, Universiti Teknologi Malaysia (UTM), Johor Bahru 81310, Malaysia; tharek@fke.utm.my (T.A.R.); abdusalamautm2017@gmail.com (A.D.)

[2] Department of Electrical Engineering, University of Malaya, 50603, Kuala Lumpur, Malaysia; nourhindia@hotmail.com (M.N.H.); effarizahanafi@um.edu.my (E.H.)

* Correspondence: ahmed.mohammed@utm.my or ahmedsecure99@gmail.com; Tel.: +60-111-162-3478

Abstract: It has been widely speculated that the performance of the next generation Internet of Things (IoT) based wireless network should meet a transmission speed on the order of 1000 times more than current wireless networks; energy consumption on the order of 10 times less and access delay of less than 1 ns that will be provided by future 5G systems. To increase the current mobile broadband capacity in future 5G systems, the millimeter wave (mmWave) band will be used with huge amounts of bandwidth available in this band. Hence, to support this wider bandwith at the mmWave band, new radio access technology (RAT) should be provided for 5G systems. The new RAT with symmetry design for downlink and uplink should support different scenarios such as device to device (D2D) and multi-hop communications. This paper presents the path loss models in parking lot environment which represents the multi-end users for future 5G applications. To completely assess the typical performance of 5G wireless network systems across these different frequency bands, it is necessary to develop path loss (PL) models across these wide frequency ranges. The short wavelength of the highest frequency bands provides many scatterings from different objects. Cars and other objects are some examples of scatterings, which represent a critical issue at millimeter-wave bands. This paper presents the large-scale propagation characteristics for millimeter-wave in a parking lot environment. A new physical-based path loss model for parking lots is proposed. The path loss was investigated based on different models. The measurement was conducted at 28 GHz and 38 GHz frequencies for different scenarios. Results showed that the path loss exponent values were approximately identical at 28 GHz and 38 GHz for different scenarios of parking lots. It was found that the proposed compensation factor varied between 10.6 dB and 23.1 dB and between 13.1 and 19.1 in 28 GHz and 38 GHz, respectively. The proposed path loss models showed that more compensation factors are required for more scattering objects, especially at 28 GHz.

Keywords: 5G; mmWave; 28 and 38 GHz; Propagation; Path Loss; IOT; D2D

1. Introduction

It is expected that mobile traffic volumes can increase a thousand times over the subsequent decade. It is expected that fifty billion devices will be connected to the network by 2020 and share information anytime and anywhere [1–3]. Due to the increasing number of connected devices, the overall capacity of the entire existing network structure needs to increase. This increasing of capacity can be done by improving energy efficiency, cost and coming up with a better system for spectrum and bandwidth utilization. Hence, better scalability options for handling the increasing number of connected devices will need to be provided. To successfully achieve the vision of increasing

the number of interconnected devices, a system has to come up with a network structure that can support up to a 1000 times increase in the projected data volume, 100 time increase in the cell capability and over a 100 times increase in the entire system capacity [3,4]. One of the key solutions for future wireless networks is device to device (D2D) communication [5,6]. With the exponential growth of mobile traffic and the improvement of local service flexibility requirements, D2D communications can alleviate the huge infrastructure investment [5]. The D2D communications allow the communication between mobile users in cellular networks directly [7]. Future 5G networks are envisaged to use resource sharing for both heavily bandwidth thirsty video applications and for handling data traffic from large cluster of sensors i.e., the so-called Internet of Things (IOT) [8–10]. It will be able to monitor and control devices with high stream of real-time information [11]. The IOT applications are enabling Machine to Machine (M2M)-driven services [8,12]. To support various IOT applications, a joint interest, physical and energy-aware cluster formation mechanism has been proposed in [8] to create clusters among the M2M devices. The adaptive clustering architecture for multimedia support in a multihop mobile network has been presented in [13]. In [12], the problem of energy and physical aware coalition formation and resource management in smart IoT applications has been addressed based on M2M communication. With the use of innovative ideas, technologies and the efficient utilization of frequency bands such as millimeter waves (mmWaves), some of the solutions can adequately meet these rising demands [14]. In fostering the development and wide spread of the fifth-generation (5G) wireless communication network, new wireless communication systems are required to offer revolution in technology with potential new spectra and novel architectural concepts [15]. As for any wireless communication system, the study of signal propagation is important for designing and modeling the 5G systems [16].

Channel characterizations at mmWave frequencies are needed in developing new standards and channel models to help engineering teams in system design and construction. The study of mmWave began as early as 1989 [17], to characterize the path loss using a low-height base station antenna in micro-cell environments at a frequency of 11 GHz. In downtown Denver, wideband non-line-of-sight (NLOS) channels at 9.6 GHz, 28.8 GHz and 57.6 GHz were measured [18]. Recently, extensive propagation measurements were conducted at frequencies of 28 GHz, 38 GHz and 73 GHz in urban microcellular and urban macro-cellular cases [19–21]. Omnidirectional path loss models in dense urban environments at frequencies of 28 GHz and 73 GHz were thoroughly investigated in [22]. Different path loss models were investigated at different frequencies between 2 GHz to 73 GHz in urban microcellular and urban macro-cellular cases [23]. The experimental channel characterizations for short distance in outdoor corridor environment using ultra-wideband channel sounder at 4.3 GHz were investigated in [24,25]. Probabilistic omnidirectional path loss models in densely populated urban areas at 28 and 73 GHz were proposed in [26]. Many measurements were conducted in parking lots at frequencies below 6 GHz [27–29]. In [30], the passive Radio Frequency Identification (RFID) tag-to-tag communication paradigm within the context of a smart parking system was adopted to improve energy-efficiency and operational effectiveness. However, to the best our knowledge, the channel characterization of mmWave bands in outdoor parking lots environment has not been reported in the literature.

In this paper, we went a step further in examining different scenarios involving 5G networks. Considering a parking lot case study, different single and multi-frequency path loss models were investigated. A new path loss model for parking lot environment that can work effectively in single and multi- frequency path loss model is proposed. For the single frequency path loss model, the close-in free space reference distance (CI) model, the floating-intercept (FI) model and parking lot path loss (PLM) proposed model were presented for single and dual parking lots environment at 28 GHz and 38 GHz frequencies. Then, they were extended to cover the multi-frequency models besides the alpha–beta–gamma (ABG) model. To show scalability of the proposed framework, some additional numerical results were provided in this work. The received power values at the transmitter

(Tx)-receiver (Rx) separation distance beyond the measurement distance are predicted based on the proposed models.

Section 2 describes the customized hardware channel measurements, the measurement locations and operating scenarios. Section 3 provides the path loss models for a single frequency. The proposed model is discussed in Section 4. Section 5 explains the path loss model for multi-frequency. The results and discussion are provided in Section 6. The conclusions are drawn in Section 7.

2. Measurement Setup and Procedure

A continuous-wave (CW) radio signal was generated by an Anritsu MG369xC Series Synthesized Signal Generator. Figure 1 shows the photograph of measurement equipment. A highly directional horn antenna vertically polarized mounted on an antenna mast was used to transmit the radio frequency signal at 28 and 38 GHz bands. The vertically polarized omni-directional receiving antenna is connected to an MS2720T spectrum analyzer operated at zero span. The Tx consisted of a single synthesized sweeper and the Rx consisted of a single spectrum analyzer. The measurement process was carried out in the parking lot next to the Scholar Inn hotel inside the Universiti Teknologi Malaysia (UTM) on the Kuala Lumpur campus as shown in Figure 2a,b. The Tx was located in a stationary position, while the Rx was moved in different locations of parking lot environment. The measurement setup was chosen to emulate the base station in wall for transmitter and as a mobile user in the receiver with height in the range of 1.3 to 1.8 m. In this measurement, the heights of the transmitting and receiving antennas above the ground level was set to 2 m and 1.7 m, respectively. The measurement setup is listed in Table 1. The single parking lot (SPL) and dual parking lot (DPL) floor plan is shown in Figure 2b. The single parking lot contained only one line of parked cars while the dual parking lot contained two parallel lines of parked cars separated by road, as shown in Figure 2b. These two scenarios were used to investigate the millimeter wave propagation in a car parking lot. The definition of SPL and DPL is addressed in Table 2. The starting point resultant distances between the transmitting and receiving antennas were 14 m and 30 m for the single and dual parking lots, respectively. During the measurement process, it was important to ensure that all objects or bodies remained at a constant stationary state to ensure that the measurement was taken as accurately as possible. The measurement was conducted when the parking lot was fully occupied by different cars, with each parking space roughly about 1.5 m width.
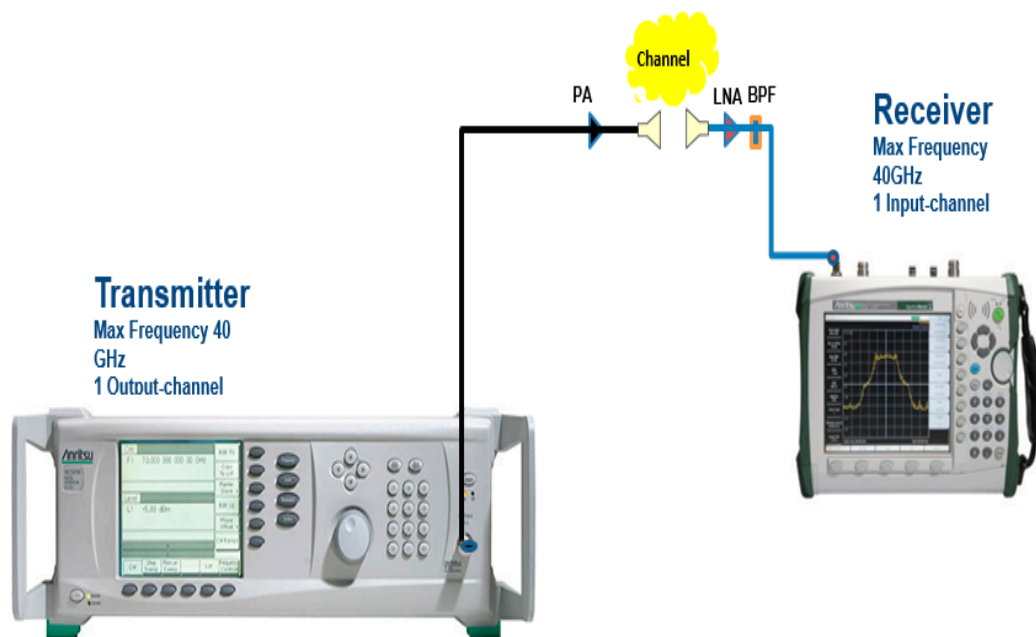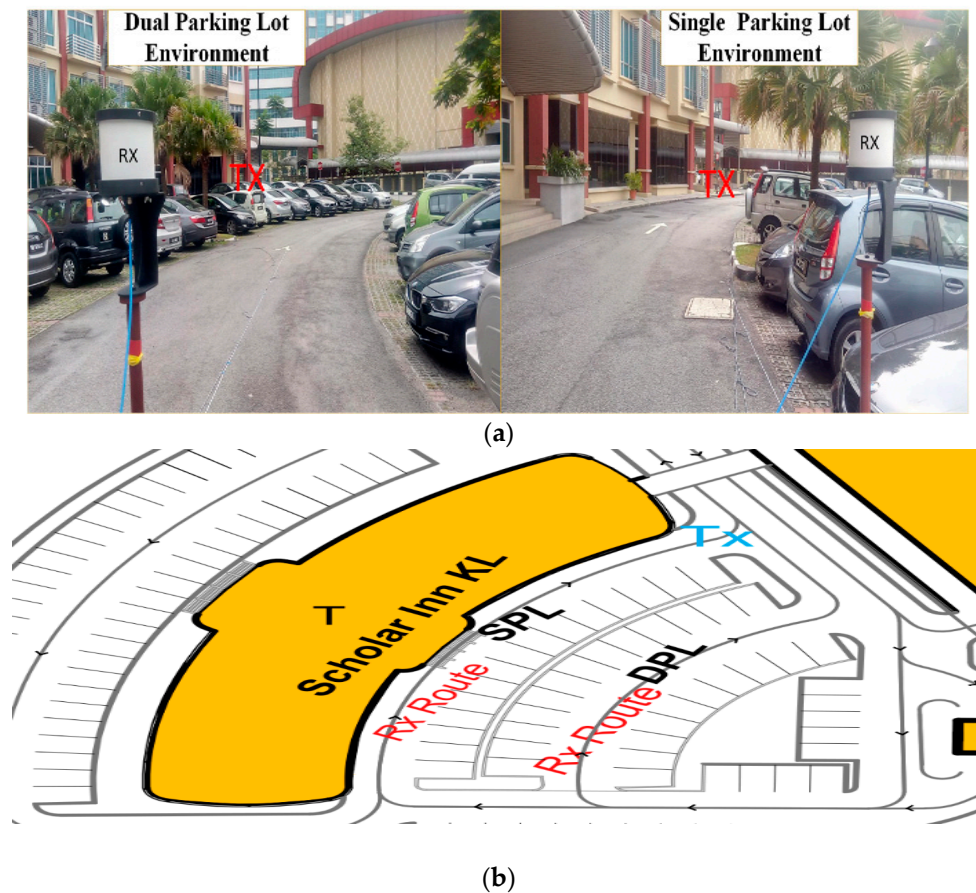

Figure 1. Measurement equipment.

(**a**)

(**b**)

Figure 2. Measurement environment: (**a**) photo of parking lots; (**b**) floor plan of the environment.

Table 1. Measurement setup parameters.

Parameter	Value
Frequency	28 GHz and 38 GHz
Transmit Power	20 dBm
Antenna Gain (28, 38 GHz)	19.18 dB, 21.10 dB
Tx Antenna Type / Beam-width (28, 38)	Horn/(18.88°, 15.23°)
Rx Antenna	Omni-directional
Tx Antenna Height	2 m
Rx Antenna Height	1.7 m

Table 2. Terminology for directional parking lots scenarios.

Setting	Description
SPL	Rx antenna was moved in one parking lot
DPL	Rx antenna was moved along two parking lots.

3. Path Loss Model for Single Frequency

Path loss (PL) is the fundamental characteristic of electromagnetic wave propagation. It is used in any wireless communication system design (i.e., link budgets) to estimate the expected Rx power [31]. The Rx power in dBm in free space can be given by the Friis transmission formula [32]:

$$P_r = \frac{P_t G_t G_r}{(4\pi d / \lambda)^2} \tag{1}$$

where P_r and P_t are the received and transmitted power, respectively. The G_t and G_r are the Tx and Rx antenna gain, respectively. The d is the link distance, and λ is wavelength for the frequency f_c. In trying to estimate path loss models, it is necessary to test for model accuracy and other path loss model parameters. Engineers will inevitably need to calculate the propagation models when designing new applications and factors like distance estimation or any other unforeseen scenarios (i.e., original forecasted or predicted in the experimental model used to determine path the loss model). Researchers are still conducting several field measurements to ensure that modeled system is stable, accurate and useful. In this paper, the 5G channel was characterized based on different path loss models for parking lot case study. Propagation path loss can be modeled using the close-in (CI) free space reference distance path loss model provided in Equation 2 with the single model parameter path loss exponent (PLE) (n):

$$PL^{CI}(f,d)[dB] = FSPL(f,d_0) + 10n \log_{10}\left(\frac{d}{d_0}\right) + \chi_\sigma^{CI} \tag{2}$$

where χ_σ^{CI} is a zero mean Gaussian random variable with standard deviation σ in dB. The free space path loss model is expressed as $FSPL(f,d_0) = \left(\frac{4\pi d}{\lambda}\right)^2$; d_0 is a physical reference distance.

Using the minimum mean square error (MMSE) [2] optimizing technique, the path loss was modeled by obtaining the PLE in CI model that matches the measured data along with the smallest error using a real-time practical reference point.

The WINNER II and 3GPP standards have been used the floating-intercept (FI) path loss model. It is not a physically-based model, as it has no anchor point constraint as with the CI model. The FI path loss model is a mathematically-based model that provides the floating-intercept (α) and line slope (β) as follow:

$$PL^{FI}(d)[dB] = \alpha + 10 \cdot \beta \log_{10}(d) + \chi_\sigma^{FI} \tag{3}$$

where χ_σ^{FI} is a zero mean Gaussian (in dB) random variable, which presents large-scale signal fluctuations about the mean path loss over a Tx-Rx separation distance. As a CI model, the MMSE is used as a best-fit that involves solving α and β to minimize σ [33].

4. Proposed Path Loss Model

The parking lot path loss model (PLM) is proposed by determining the compensation factors for single and dual parking lots, where the path loss exponent value was set to 2 as a free space path loss exponent. The path loss exponent was set to 2 to model the propagation of the 5G channel based on the effect of reflection from cars and other objects in the measurement environment. This model was extracted with respect to 1 m reference; thus, it is a physical-based model and it is defined as:

$$PL^{PLM}(f,d)[dB] = FSPL(f,d_0) + 10n \log_{10}\left(\frac{d}{d_0}\right) + k_f + \chi_\sigma^{PLM} \tag{4}$$

where n is the free space path loss exponent of 2, k_f is giving as the path compensation factor with respect to number of the parking lot and χ_σ^{PLM} is the shadowing factor with standard deviation (σ) in dB. With N number of data points, the MMSE was used to estimate the k_f and minimum standard deviation as follows:

$$\chi_\sigma^{PLM} = PL^{PLM}(d)[dB] - FSPL(f,d_0) - 10n \log_{10}\left(\frac{d}{d_0}\right) - k_f = Z - S - k_f, \tag{5}$$

where $Z = PL^{PLM}(d)[dB] - FSPL(f,d_0)$ and $S = 20 \log_{10}\left(\frac{d}{d_0}\right)$.

The standard deviation σ^{PLM} for the PLM model becomes:

$$\sigma^{PLM} = \sqrt{\frac{\sum \chi_\sigma^{PLM^2}}{N}} = \sqrt{\frac{\sum (Z - S - k_f)^2}{N}} \tag{6}$$

In order to minimize σ^{PLM}, the term $(Z - S - k_f)^2$ should be minimized by making the derivative of $(Z - S - k_f)^2$ with respect to k_f zero, such that:

$$\frac{\partial \sum (Z-S-k_f)^2}{\partial k_f} = \sum 2(k_f + S - Z) = 2(k_f \times N + \sum S - \sum Z) =$$
$$2(k_f \times N + \frac{\sum SZ \sum S}{\sum S^2} - \sum Z) = 0 \tag{7}$$

From (7):

$$k_f = \frac{\sum Z}{N} - \frac{\sum SZ \sum S}{N \sum S^2} \tag{8}$$

Therefore, the minimum standard deviation for the PLM proposed model is:

$$\sigma^{PLM}_{\min} == \sqrt{(S - S\frac{\sum SZ}{S^2} - \frac{\sum Z}{N} + \frac{\sum SZ \sum S}{N \sum S^2})^2 / N} \tag{9}$$

The Z and S can be considered column vectors and the optimum k_f can also be expressed in matrix form as:

$$k_f = \sqrt{(\sum Z - (Z^T(S^TS)^{-1}S)\sum S)/N} \tag{10}$$

where the $(.)^T$ operator represents the transpose of the column vector.

5. Path Loss Model for Multi-Frequency

Multi-frequency path loss models were proposed to broad the frequencies and measurements range. The ABG model was used for path losses at various frequencies (multi-frequency model). Additionally, the CI and PLM models were used for both single and multi-frequency data sets. In our proposed study, the ABG model had a 1 m reference distance and 1 GHz reference frequency (f_0 set to 1 GHz). The ABG model equation is given as [34]:

$$PL^{ABG}(f,d)[dB] = 10\alpha \log_{10}\left(\frac{d}{d_0}\right) + \beta + 10\gamma \log_{10}\left(\frac{f}{f_0}\right) + \chi_\sigma^{ABG} \tag{11}$$

where α and γ are constant coefficients; these coefficients are majorly used to indicate the dependencies of frequency and distance on path loss, β is referred to as offset in path loss, f is frequency in GHz and χ_σ^{ABG} is a Gaussian random variable. As for the CI model, the ABG model parameters were calculated using the MMSE approach.

6. Results and Discussions

Path Loss Models Results

Figure 3 shows that the path loss at 28 GHz increased as the separation distance increased; this observation was the same for both single and dual parking lots. The path loss observed in the DPL was much more than in the SPL by an average value of about 7 dB/decade. Using the CI path loss model, the path loss exponent values were 2.7 and 3.4 for SPL and DPL, respectively, as shown in Figure 3. Comparing with FSPL exponent of 2, the path loss values obtained from the parking lot indicate that the most experienced losses were due to the car objects. In the SPL, the PLE obtained values that indicate 7 dB/decade for the signal drop, which doubled (14 dB/decade) for DPL, as shown in Figure 3. The standard deviation values for both scenarios were approximately identical, which means that the shadowing effect for both scenarios was nearly the same. For the 38 GHz band, it can be shown that the PLE for the DPL was greater than the SPL by 3 dB/decade, as shown in Figure 4. The PLE values were 2.8 and 3.1 for SPL and DPL, respectively. Comparing Figures 3 and 4, it can be shown that the PLEs were approximately identical for 28 GHz and 38 GHz bands for a SPL. However, the losses in the 28 GHz band were greater than the 38 GHz for the DPL by 3 dB/decade. This result indicates that

some of the paths losses at 28 GHz were added up destructively, which caused the degradation of the power level which appears clearly from the distance range from 40 to 50 m, where the path loss at 28 GHz degraded by 10 dB as compared to the 38 GHz at the same range distance.
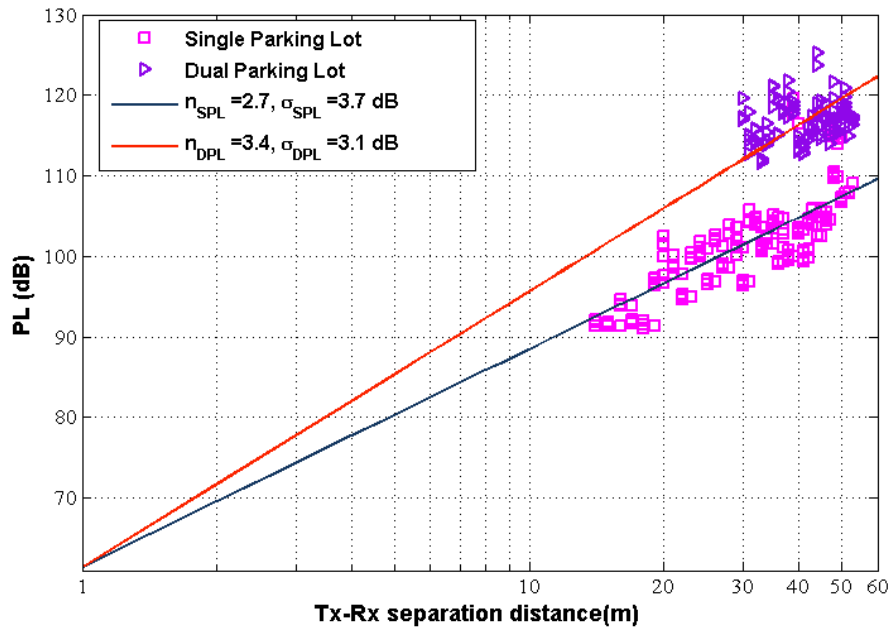

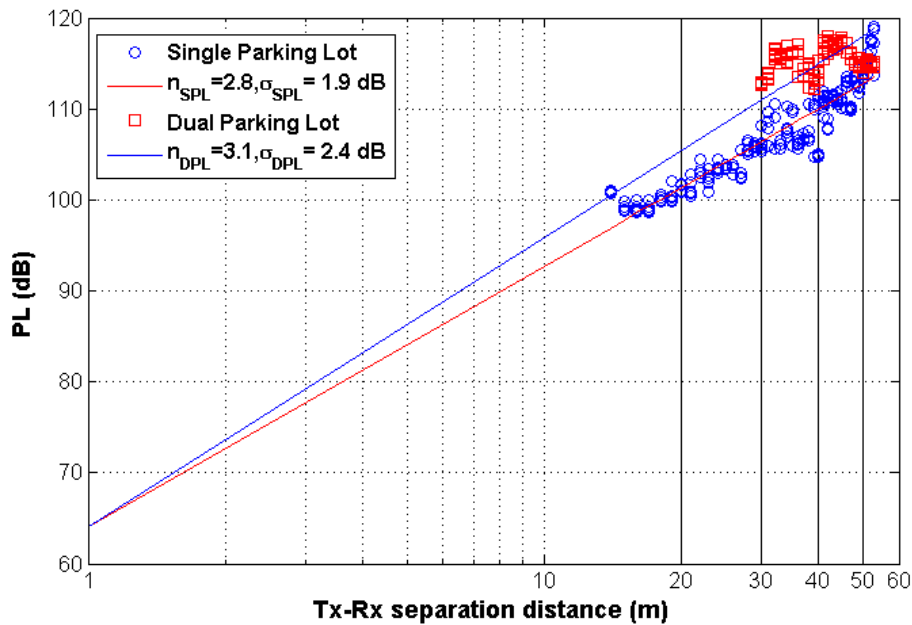**Figure 3.** Close-in (CI) free space reference distance path loss model at 28 GHz.

Figure 4. CI path loss model at 38 GHz.

For the FI path loss model, Figures 5 and 6 show the PL models with respect to the separation distance at 28 GHz and 38 GHz. For 28 GHz, the FI path loss model parameters show that the PLE (*B* slope) value was approximately identical to the CI model with 3 dB less for the SPL scenario. Additionally, the value was comparable with that of 1 m separation distance, which was lower than the theoretical one by only 4.3 dB. The FI slope values at 38 GHz and 28 GHz for DPL were low as compared to the CI model at 28 GHz and 38 GHz. The reason for this observation is because of small difference between the reference value at 30 m and the maximum FI PL value at 50 m. This implies that the slope of the PL was low, whereas, in the CI model (the reference value is at 1 m), the slope

along the PL was large with respect to 50 m PL value. It can be concluded that the FI model showed a tight reflection frequency dependency at 28 GHz and 38 GHz as shown in Figures 5 and 6, respectively. This effect can be described as a wavelength effect, since, if there is a reduction in wavelength, there will be a proportional increase in the rate of reflection. In conclusion, the FI model can be used as an effective model for DPL, and it is highly recommended at the 38 GHz frequency band.
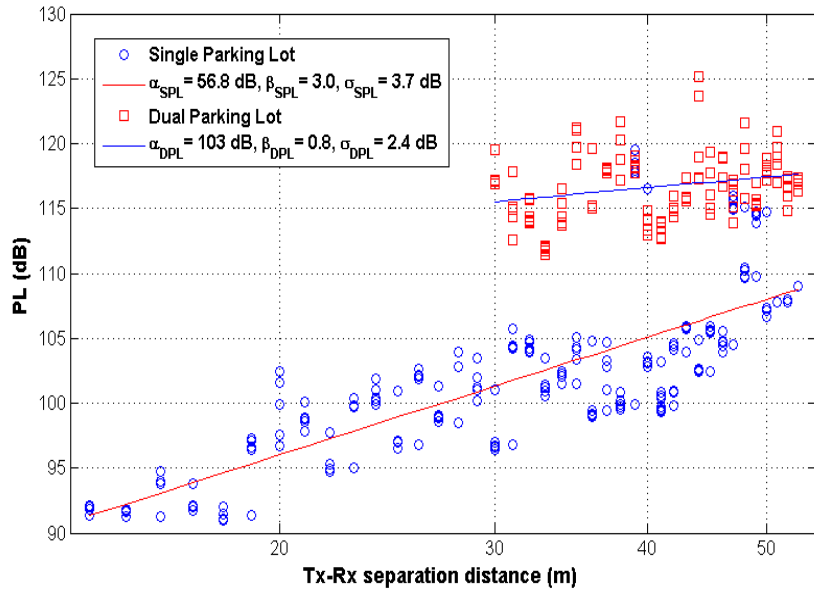

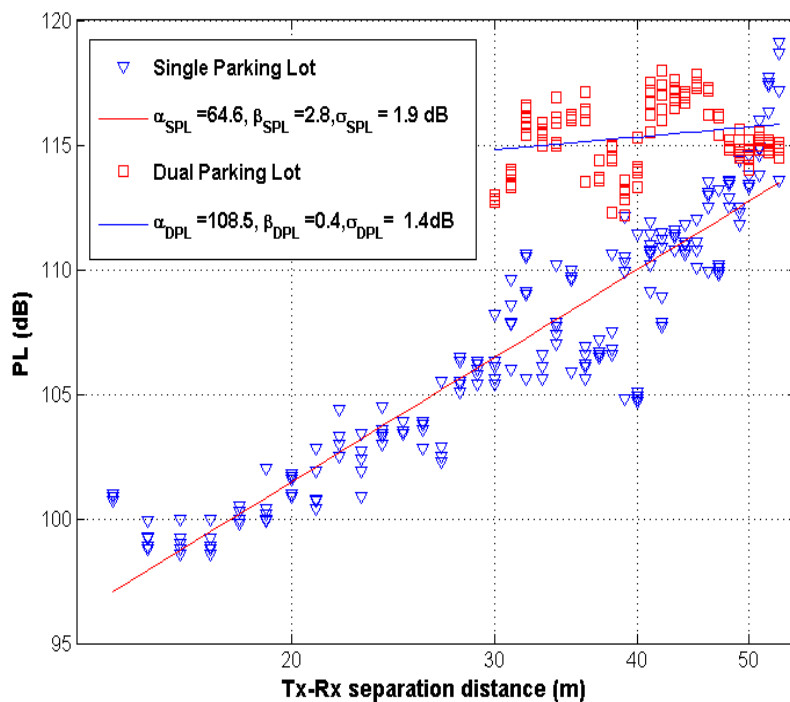**Figure 5.** Floating-intercept (FI) path loss model at 28 GHz.

Figure 6. FI path loss model at 38 GHz.

Figures 7 and 8 show the proposed PLM path loss model at 28 GHz and 38 GHz for the SPL and DPL scenarios. It can be shown that for the parking lot factor k_f values of 28 GHz were 10.6 dB and 23.1 dB for SPL and DPL, respectively, as depicted in Figure 7. This indicates that the power decay for the DPL was twice that of the SPL at 28 GHz band. Figure 8 shows that the parking lot factor values of 38 GHz are 13.1 dB and 19.1 dB for SPL and DPL, respectively. At 38 GHz band, the effect of the DPL

was less than the effect at 28 GHz, where the power decay is 6 dB over the SPL, as shown in Figure 8. This implies that the reflection was better and there was less shadowing effect at 38 GHz compared to the 28 GHz band. The standard deviation values show that the effect at 38 GHz bands was half that of the standard deviation values at 28 GHz band. The parameters of the proposed path loss models are listed in Table 3. Hence, it can be concluded that the proposed model was a physical-based model (accurate model) and a simple model: only one parameter needs to be estimated, which is the parking lot loss factor k_f. The k_f factor provided the effect of parking lot using a PLE of 2 (FSPL exponent) for different frequencies.
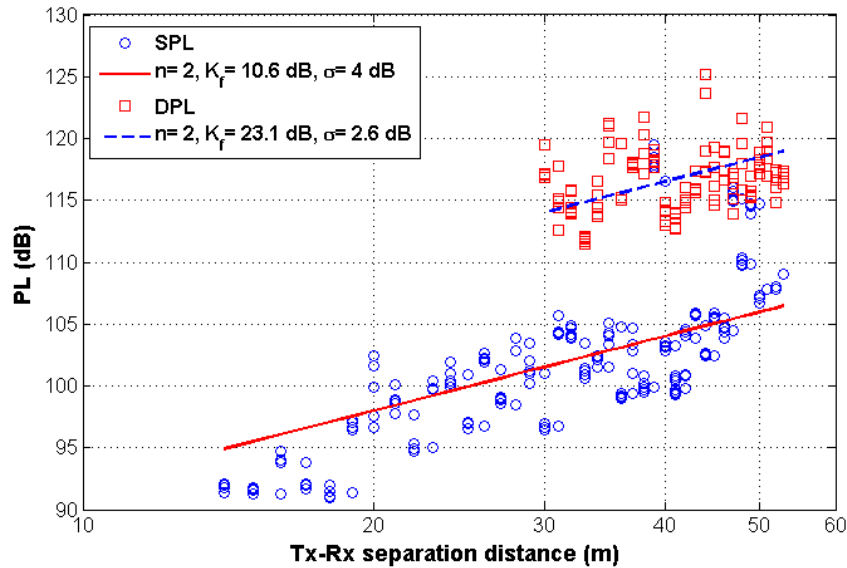

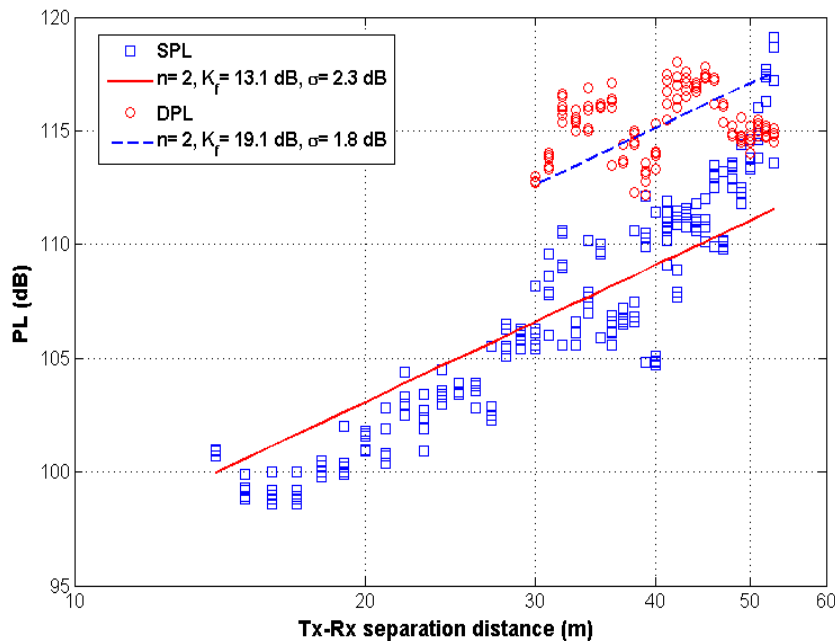**Figure 7.** The proposed parking lot path loss model (PLM) at 28 GHz.

Figure 8. The proposed PLM at 38 GHz.

Table 3. The PLM for 28GHz and 38 GHz.

Scenario	Frequency (GHz)	# of Data Point	Dist. Range (m)	n^{CI}	σ^{CI}(dB)	k_f
SPL	28 GHz	201	14–53	2	4.0	10.6
DPL		187	30–66	2	2.6	23.1
SPL	38 GHz	201	14–53	2	2.3	13.1
DPL		187	30–66	2	1.8	19.1

In addition to the FI path loss model, the ABG models were proposed as multi-frequency path loss model with three main parameters. As shown in Table 4, the three-parameter ABG model had the lowest standard deviation in DPL compared to the SPL by 1 dB. The distance dependent factor α values in DPL and SPL were 0.6 and 2.9, respectively. The frequency dependent factor γ values were 3.8 and 0.9 for SPL and DPL, respectively. This significant difference in value of slope indicates that more constructive reflections that in DPL as compared to SPL case study. Even though the DPL showed higher performance than the SPL, it was at the expense of an additional optimization factor by roughly 120 dB as compared to the SPL. The reason behind the optimization factor difference can be expected, since some path loss values for the DPL had a high difference compared to mean DPL path loss values as shown in Figure 9. The three-parameter ABG model can typically obtain an additional accuracy comparing with other models at the expense of complexity. The CI path loss model was also used for multi-frequencies. Table 4 shows the PLEs were 2.8 and 3.3 for CI model at SPL and DPL scenarios, respectively. It can be noted that these values are comparable with CI in the single frequency case study. The standard deviation shows close values to CI-28 GHz in the single frequency case study. Table 4 lists the parameters of the proposed models for multi-frequencies. The results of the PLM proposed model for multi-frequency show that the additive factor for the DPL was two times larger than the SPL, which means the proposed model was accurately working at multi-frequency. The k_f factor values were 11.8 dB and 21.1 dB for SPL and DPL, respectively. The standard deviation values were 3 dB and 5 dB for SPL and DPL, respectively.
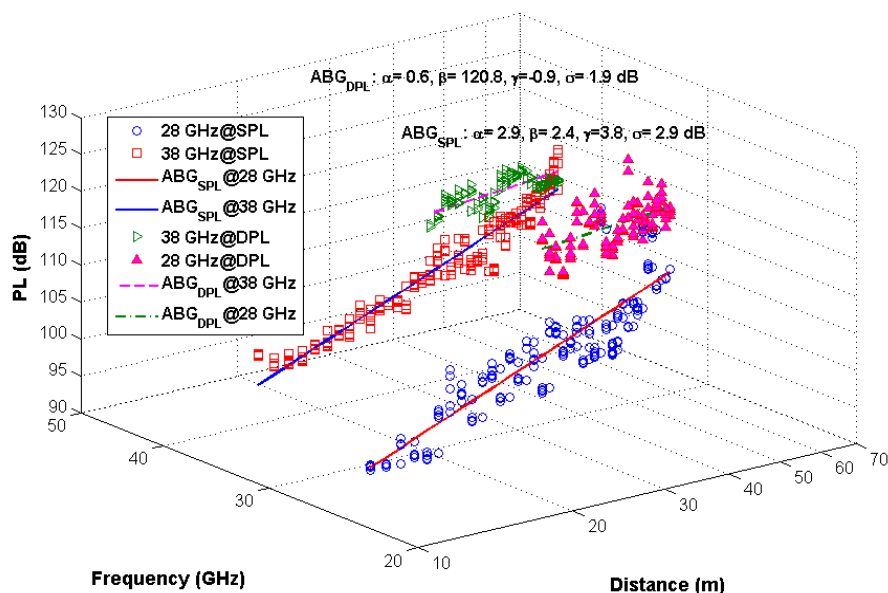

Figure 9. The alpha-beta-gamma (ABG) path loss model for 28 GHz and 38 GHz. 6.2 Numerical Results and Computation Complexity.

Table 4. Multi-frequency path loss model for 28 GHz and 38 GHz.

Scenario	Model	*n*	*α*	*b*	*γ*	*Kf*	*σ* [dB]
SPL	ABG	-	2.9	2.4	3.8	-	2.9
DPL		-	0.6	120.8	0.9	-	1.9
SPL	CI	2.8	-	-	-	-	3.2
DPL		3.3	-	-	-	-	3.4
SPL	PLM	2	-	-	-	11.8 dB	3.0
DPL		2	-	-	-	21.1 dB	3.5

To show scalability of the proposed framework, some additional numerical results are provided in this section. Figures 10 and 11 show the predicted received power at 28 and 38 GHz, respectively. This was calculated based on proposed path loss models in this work at Tx power of 25 dBm. The received power values were calculated at the Tx-Rx separation distance beyond the measurement distance. The received power presents ratio of the transmitted power to the path loss. The predicted received power at different Tx-Rx separation distance is presented in Table 5 at 28 GHz and 38 GHz bands for SPL and DPL scenarios. The complexity for the path loss models was evaluated based on the number of estimated parameters using MMSE approach [2]. The PLM proposed model and CI model outperformed the FI and ABG models in terms of computation complexity. For the PLM and CI models, only one parameter for each one was required to be estimated by the MMSE approach, which were *n* and k_f, for CI and PLM respectively. The FI path loss model has two parameters ($α$ and $β$) which were estimated by MMSE. The computation complexity of ABG model was the highest one, where three parameters ($α$, $β$ and Y) needed to be estimated using MMSE. In conclusion, the complexity of FI and ABG models are two and three times more than the complexity of PLM and CI models, respectively.
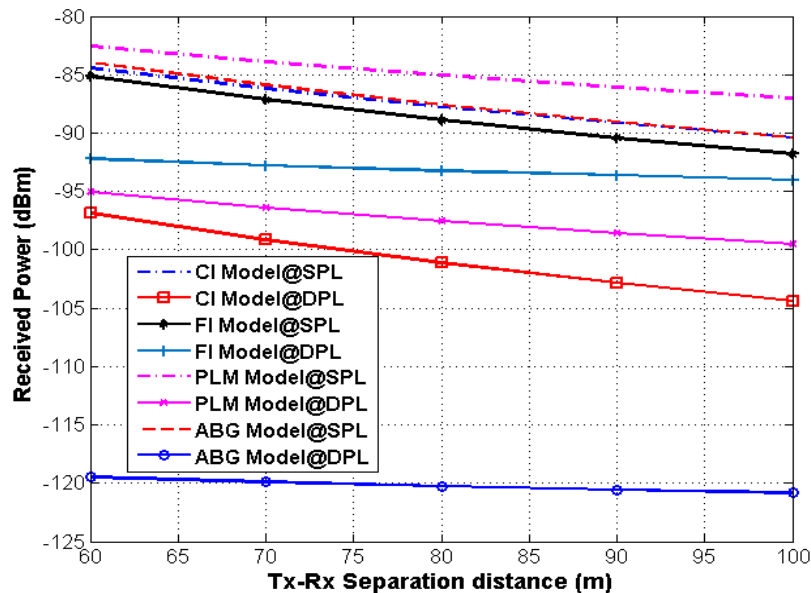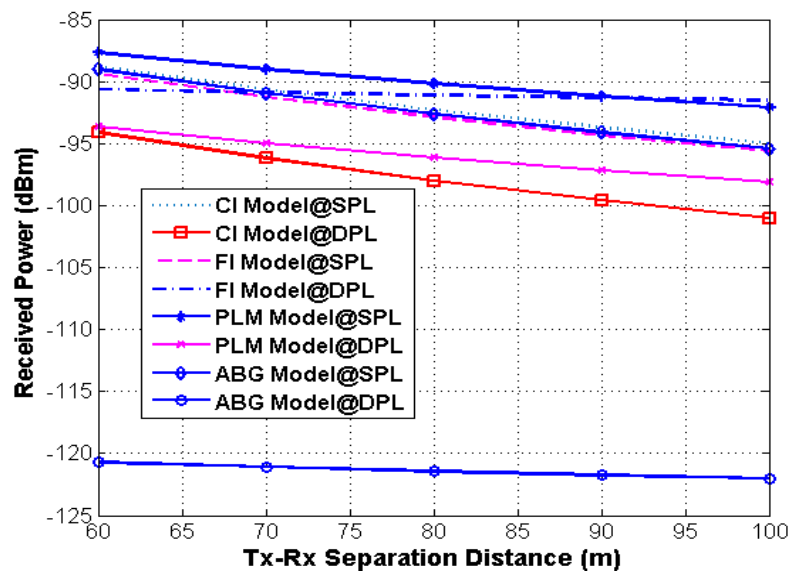

Figure 10. Predicted received power at 28 GHz.

Figure 11. Predicted received power at 38 GHz.

Table 5. Received power at different transmitter (Tx)-receiver (Rx) separation distance using all studied path loss models.

Tx-Rx Separation Distance (m)	Path Loss Models	Frequency (GHz)	Scenarios	Power Received (P_r) (dBm) = P_t-PL
60, 70, 80, 90, 100	CI	28	SPL	−84.4, −86.2, −87.8, −89.2, −90.4
			DPL	−96.9, −99.1, −101.11, −102.8, −104.4
		38	SPL	−88.8, −90.7, −92.3, −93.7, −95.0
			DPL	−94.12, −96.2, −98.0, −99.6, −101.0
60, 70, 80, 90, 100	FI	28	SPL	−85.1, −87.2, −88.9, −90.4, −91.9
			DPL	−92.2, −92.8, −93.2, −93.6, −94
		38	SPL	−89.4, −91.3, −92.9, −94.3, − 95.6
			DPL	−90.6, −90.9, −91.1, −91.3, −91.5
60, 70, 80, 90, 100	PLM	28	SPL	−82.6, −83.9, −85.1, −86.1, −87
			DPL	−95.1, −96.4, −97.6, −98.6, −99.5
		38	SPL	−87.7, −89, −90.2, −91.2, −92.1
			DPL	−93.7, −95, −96.2, −97.2, −98.1
60, 70, 80, 90, 100	ABG	28	SPL	−94, −85.9, −87.6, −89.1, −90.4
			DPL	−119.5, −119.9, −120.2, −120.5, −120.8
		38	SPL	−89.0, −90.9, −92.6, −94.1, −95.4
			DPL	−120.7, −121.1, −121.4, −121.7, −122

7. Conclusions

In this paper, large-scale propagation measurement was carried out in a parking lot to study the path loss for 5G over the 28 GHz and 38 GHz candidate bands. These two different frequencies bands were studied in terms of signal losses across different modeled scenarios in a fully pack parking lots. For the single frequency path loss model, the CI-PLEs were approximately identical in the 28 GHz and 38 GHz bands for a single and dual parking lot. The PLE of the 38 GHz band was larger than the 28 GHz by only 1dB/decade and 3 dB/decade for SPL and DPL, respectively. The FI model showed a tight reflection frequency dependency at 28 GHz and 38 GHz. The 28 GHz slope line value was larger than the slope line at 38 GHz. It represents the wavelength effect, since, as the wavelength was smaller at 38 GHz, the reflection was larger. Thus, the FI model is recommended to be used as a model when considering DPL environments; the recommended frequency is 38 GHz. For the PLM proposed model, the compensation factor for the 28 GHz band was 10.6 dB and 23.1 dB for single and dual parking lot, respectively. This indicates that the power decay for the double-parking lot was twice as large as that of the single parking lot at a 28 GHz band.

It can be concluded that for the 38 GHz band, the effect of the double-parking lot was less, whereas the power decay was 6 dB in the single parking lot. This shows that the reflection is better and there is a very small shadow effect at 38 GHz when compared to the 28 GHz frequency band. The standard deviation values also showed that the effects at the 38 GHz band were half of those at the 28 GHz band.

This work investigated the path loss in parking lots at 28 GHz and 38 GHz. For this study, the narrowband system was used to conduct the measurement. It is powerful system for the path loss models, as the total power concentrate at the center frequency. However, the delay spread and angular spread cannot be detected. For future work, the wideband channel sounder will be used within a 1 GHz bandwidth, where the delay and angular spreads can be extracted from multipath components. In wideband measurement, we can distinguish between multipath components with an 1 ns resolvable delay bin. Moreover, the PLM proposed model will be investigated in underground and proximity parking lot environments.

Author Contributions: Conceptualization, A.M.A.-S., T.A.R., A.D. and E.H.; Data curation, A.M.A.-S. and M.N.H.; Formal analysis, A.M.A.-S., M.N.H., A.D. and E.H.; Funding acquisition, T.A.R.; Investigation, A.M.A.-S., T.A.R. and M.N.H.; Methodology, A.M.A.-S., T.A.R. and M.N.H.; Project administration, T.A.R.; Resources, A.M.A.-S., T.A.R. and E.H.; Software, A.M.A.-S.; Supervision, T.A.R.; Validation, A.M.A.-S. and T.A.R.; Visualization, A.M.A.-S. and A.D.; Writing—original draft, A.M.A.-S.; Writing—review & editing, A.M.A.-S., T.A.R., M.N.H., A.D. and E.H.

Conflicts of Interest: The authors declare no conflict of interest.

References

1. Osseiran, A.; Boccardi, F.; Braun, V.; Kusume, K.; Marsch, P.; Maternia, M.; Queseth, O.; Schellmann, M.; Schotten, H.; Taoka, H.; et al. Scenarios for 5G mobile and wireless communications: the vision of the METIS project. *IEEE Commun. Mag.* **2014**, *52*, 26–35. [CrossRef]

2. Al-Samman, A.M.; Rahman, T.A.; Azmi, M.H.; Hindia, M.N.; Khan, I.; Hanafi, E. Statistical modelling and characterization of experimental mm-wave indoor channels for future 5G wireless communication networks. *PLoS ONE* **2016**, *11*, e0163034. [CrossRef] [PubMed]

3. Rangan, S.; Rappaport, T.S.; Erkip, E. Millimeter-wave cellular wireless networks: Potentials and challenges. *Proc. IEEE* **2014**, *102*, 366–385. [CrossRef]

4. Gupta, A.; Jha, R.K. A survey of 5G network: Architecture and emerging technologies. *IEEE Access* **2015**, *3*, 1206–1232. [CrossRef]

5. Katsinis, G.; Tsiropoulou, E.E.; Papavassiliou, S. Joint resource block and power allocation for interference management in device to device underlay cellular networks: A game theoretic approach. *Mob. Netw. Appl.* **2017**, *22*, 539–551. [CrossRef]

6. Shen, X. Device-to-device communication in 5G cellular networks. *IEEE Netw.* **2015**, *29*, 2–3. [CrossRef]

7. Tehrani, M.N.; Uysal, M.; Yanikomeroglu, H. Device-to-device communication in 5G cellular networks: Challenges, solutions, and future directions. *IEEE Commun. Mag.* **2014**, *52*, 86–92. [CrossRef]

8. Tsiropoulou, E.E.; Mitsis, G.; Papavassiliou, S. Interest-aware energy collection & resource management in machine to machine communications. *Ad. Hoc. Networks* **2018**, *68*, 48–57. [CrossRef]

9. Cero, E.; Baraković Husić, J.; Baraković, S. IoT's tiny steps towards 5G: Telco's perspective. *Symmetry* **2017**, *9*, 213. [CrossRef]

10. Chiu, W.; Su, C.; Fan, C.; Chen, C.; Yeh, K.H. Authentication with what you see and remember in the internet of things. *Symmetry* **2018**, *10*, 537. [CrossRef]

11. Parada, R.; Cárdenes-Tacoronte, D.; Monzo, C.; Melià-Seguí, J. Internet of Things Area Coverage Analyzer (ITHACA) for complex topographical scenarios. *Symmetry* **2017**, *9*, 237. [CrossRef]

12. Tsiropoulou, E.E.; Paruchuri, S.T.; Baras, J.S. Interest, energy and physical-aware coalition formation and resource allocation in smart IoT applications. In Proceedings of the 2017 51st Annual Conference on Information Sciences and Systems (CISS), Baltimore, MD, USA, 22–24 March 2017; pp. 1–6.

13. Lin, C.R.; Gerla, M. Adaptive clustering for mobile wireless networks. *IEEE J. Sel. Areas Commun.* **1997**, *15*, 1265–1275. [CrossRef]

14. Rappaport, T.S.; Mayzus, R.; Azar, Y.; Wang, K.; Wong, G.N.; Schulz, J.K.; Samimi, M.; Gutierrez, F. Millimeter wave mobile communications for 5G cellular: It will work! *IEEE Access* **2013**, *1*, 335–349. [CrossRef]

15. Boccardi, F.; Heath, R.; Lozano, A.; Marzetta, T.L.; Popovski, P. Five disruptive technology directions for 5G. *IEEE Commun. Mag.* **2014**, *52*, 74–80. [CrossRef]

16. Shariat, M.; Gutierrez-Estevez, D.M.; Vijay, A.; Safjan, K.; Rugeland, P.; da Silva, I.; Lorca, J.; Widmer, J.; Fresia, M.; Li, Y.; et al. 5G radio access above 6 GHz. *Trans. Emerg. Telecommun. Technol.* **2016**, *25*, 294–307. [CrossRef]

17. Rappaport, T.S. Characterization of UHF multipath radio channels in factory buildings. *IEEE Trans. Antennas Propag.* **1989**, *37*, 1058–1069. [CrossRef]

18. Violette, E.J.; Espeland, R.H.; DeBolt, R.O.; Schwering, F.K. Millimeter-wave propagation at street level in an urban environment. *IEEE Trans. Geosci. Remote Sens.* **1988**, *26*, 368–380. [CrossRef]

19. Sun, S.; Rappaport, T.S.; Rangan, S.; Thomas, T.A.; Ghosh, A.; Kovacs, I.Z.; Rodriguez, I.; Koymen, O.; Partyka, A.; Jarvelainen, J. Propagation path loss models for 5G urban micro- and macro-cellular scenarios. In Proceedings of the 2016 IEEE 83rd Vehicular Technology Conference (VTC Spring), Nanjing, China, 15–18 May 2016; pp. 1–6.

20. Thomas, T.A.; Rybakowski, M.; Sun, S.; Rappaport, T.S.; Nguyen, H.; Kovács, I.Z. A prediction study of path loss models from 2-73.5 GHz in an urban-macro environment. In Proceedings of the 2016 IEEE 83rd Vehicular Technology Conference (Spring VTC-2016), Nanjing, China, 15–18 May 2016; pp. 1–5.

21. Nossire, Z.; Gupta, N.; Almazaydeh, L.; Xiong, X. New empirical path loss model for 28 GHz and 38 GHz millimeter wave in indoor urban under various conditions. *Appl. Sci.* **2018**, *8*, 2122. [CrossRef]

22. MacCartney, G.R.; Samimi, M.K.; Rappaport, T.S. Omnidirectional path loss models in New York City at 28 GHz and 73 GHz. In Proceedings of the 2014 IEEE 25th Annual International Symposium on Personal, Indoor, and Mobile Radio Communication (PIMRC), Washington, DC, USA, 2–5 September 2014; pp. 227–231.

23. Sun, S.; Rappaport, T.S.; Thomas, T.A.; Ghosh, A.; Nguyen, H.C.; Kovacs, I.Z.; Rodriguez, I.; Koymen, O.; Partyka, A. Investigation of prediction accuracy, sensitivity, and parameter stability of large-scale propagation path loss models for 5G wireless communications. *IEEE Trans. Veh. Technol.* **2016**, *65*, 2843–2860. [CrossRef]

24. Al-Samman, A.M.; Rahman, T.A.; Nunoo, S.; Chude-Okonkwo, U. a. K.; Ngah, R.; Shaddad, R.Q.; Zahedi, Y. Experimental characterization and analysis for ultra wideband outdoor channel. *Wirel. Pers. Commun.* **2015**, *83*, 3103–3118. [CrossRef]

25. Al-Samman, A.M.; Rahman, T.A. Experimental characterization of multipath channels for ultra-wideband systems in indoor environment based on time dispersion parameters. *Wirel. Pers. Commun.* **2017**, *95*, 1713–1724. [CrossRef]

26. Samimi, M.K.; Rappaport, T.S.; MacCartney, G.R. Probabilistic omnidirectional path loss models for millimeter-wave outdoor communications. *IEEE Wirel. Commun. Lett.* **2015**, *4*, 357–360. [CrossRef]

27. Jang, J.S.; Yim, H.Y.; Lee, K.B. Channel prediction-based user selection algorithm for multiuser environments. In Proceedings of the 2010 International Conference on Information and Communication Technology Convergence (ICTC), Jeju, Korea, 17–19 November 2010; pp. 239–240.

28. Matolak, D.W.; Sun, R.; Liu, P. V2V channel characteristics and models for 5 GHz parking garage channels. In Proceedings of the 2015 9th European Conference on Antennas and Propagation (EuCAP), Lisbon, Portugal, 13–17 April 2015; pp. 1–4.

29. Santos, T.; Karedal, J.; Almers, P.; Tufvesson, F.; Molisch, A. Modeling the ultra-wideband outdoor channel: Measurements and parameter extraction method. *IEEE Trans. Wirel. Commun.* **2010**, *9*, 282–290. [CrossRef]

30. Tsiropoulou, E.E.; Baras, J.S.; Papavassiliou, S.; Sinha, S. RFID-based smart parking management system. *Cyber-Phys. Syst.* **2017**, *3*, 22–41. [CrossRef]

31. Al-Samman, A.M.; Rahman, T.A.; Azmi, M.H.; Hindia, M.N. Large-scale path loss models and time dispersion in an outdoor line-of-sight environment for 5G wireless communications. *AEU-Int. J. Electron. Commun.* **2016**, *70*, 1515–1521. [CrossRef]

32. Rappaport, T.S. *Wireless Communications Principles and Practice*, 2nd ed.; Prentice Hall Communications Engineering and Emerging Technologies Series; Prentice Hall: Upper Saddle River, NJ, USA, 2002.

33. MacCartney, G.; Rappaport, T.; Sun, S.; Deng, S. Indoor office wideband millimeter-wave propagation measurements and channel models at 28 GHz and 73 GHz for ultra-dense 5G wireless networks. *IEEE Access* **2015**, *3*, 2388–2424. [CrossRef]
34. Al-Samman, A.M.; Rahman, T.A.; Azmi, M.H. Indoor corridor wideband radio propagation measurements and channel models for 5G millimeter-wave wireless communications at 19 GHz, 28 GHz and 38 GHz bands. *Wirel. Commun. Mob. Comput.* **2018**, *2018*, 1–12. [CrossRef]